Q. J. R. Meteorol. Soc. (1991), **117**, pp. 107–124 551.515.21

A numerical study of tropical cyclone motion using a barotropic model. II: Motion in spatially-varying large-scale flows

By WOLFGANG ULRICH and ROGER K. SMITH

Meteorologisches Institut, Universität München, Theresienstr. 37, 8000 *München* 2, *F.R.G.*

(Received 12 September 1989, revised 29 May 1990)

SUMMARY

The motion of an initially symmetric vortex in a spatially-varying large-scale flow on a beta plane is investigated using a nondivergent, barotropic numerical model. The calculations extend those carried out for the case of zero basic flow in Part I. The large-scale flows are provided by meridionally-varying zonal flows, or single-mode, stationary, finite-amplitude planetary waves in a channel. Interest is focused on the evolution of vortex asymmetries and their role in determining vortex motion relative to the basic large-scale flow.

As in Part I, the calculations are used to assess averaging procedures for computing the environmental wind field of a tropical cyclone from observed wind data. It is shown that averaging over an annular region centred on the vortex is, in principle, more accurate when there is a basic flow, in comparison with the case of zero basic flow.

1. INTRODUCTION

In Part I (Smith *et al.* 1990) we investigated the dynamics of initially symmetric and asymmetric vortices on a beta plane with no imposed flow, using a barotropic numerical model. In this companion paper we use the model to study vortex motion in spatially-varying large-scale flows. The formulation has been designed to focus on flows that are relevant to the important problem of understanding tropical cyclone recurvature. The large-scale flows are provided by single-mode, finite-amplitude planetary wave solutions to the barotropic vorticity equation in a zonal channel, or simply to zonally-independent flows with linear, quadratic or sinusoidal profiles in the meridional direction, the latter being the limiting case of a planetary wave with zero zonal wavenumber.

Of special interest is the evolution of the so-called beta gyres, discussed in Part I and elsewhere, in comparison with the case of zero motion and constant absolute vorticity gradient of the basic state. In particular, we investigate the structure of the vortex asymmetries as the vortex undergoes recurvature from lower-latitude easterlies to higher-latitude westerly winds and study the conditions under which recurvature occurs.

In Part I we showed that, using a method of partitioning the flow between vortex and environment introduced by Kasahara and Platzman (1963; their Method III), the environmental streamflow provides a 'steering current' for the vortex to a very close approximation. The generality of this result when there is a non-zero basic flow is explored. Moreover, as in Part I, we investigate the possibility of 'retrieving' this steering current by averaging the total wind over an annular region surrounding the cyclone, a procedure used in observational studies.

2. MODEL FORMULATION

The basic model is described in Part I. Calculations are based on the solution of the non-divergent vorticity equation which, in terms of the streamfunction ψ can be written

$$\frac{\partial}{\partial t}\nabla^2\psi + J(\psi, \nabla^2\psi) + \beta\frac{\partial \psi}{\partial x} = 0 \tag{2.1}$$

where J is the Jacobian operator, and other notation is as defined in Part I. The

computational domain is a rectangle $-2L \leq x \leq 2L$, $-L \leq y \leq L$ with channel boundary conditions

$$\frac{\partial \psi}{\partial x} = 0 \quad \text{at } y = \pm L \tag{2.2}$$

and periodic boundary conditions at $x = \pm 2L$.

An elementary, but exact solution of Eq. (2.1) subject to these boundary conditions is $\psi = \overline{\psi}(y)$, where $\overline{u}(y) = -(\partial \overline{\psi}/\partial y)$ is an arbitrary zonal flow. There exist also *exact* solutions for finite-amplitude planetary wave modes on a uniform zonal current with speed U of the form:

$$\overline{\psi}(x, y, t) = U(L - y) + \hat{\psi} \cos(kx + U_d t + \alpha) \cos ly \tag{2.3}$$

where k and l are integer multiples of π/L and $\pi/2L$, respectively,

$$U_d = -U + \beta/(k^2 + l^2) \tag{2.4}$$

is the westward drift speed of the mode, and $\hat{\psi}$ and α are constants characterizing the wave amplitude and phase, respectively.

Equation (2.1) is initialized by adding the symmetric vorticity distribution $\zeta_0(|\mathbf{x} - \mathbf{x}_0|)$, corresponding with a velocity distribution $V(|\mathbf{x} - \mathbf{x}_0|)$, to the vorticity field of one of the above basic flows. Here, $\mathbf{x} = (x, y)$ is the position vector of a point in the flow and $\mathbf{x}_0$ is the initial location of the symmetric vortex centre. In all cases we have used the tangential wind profile shown in Fig. 1. of Part I for V. Equation (2.1) is integrated forward in time using the finite difference method described in Part I. As usual, vorticity ζ and streamfunction ψ are related by the equation

$$\nabla^2 \psi = \zeta. \tag{2.5}$$

In the present calculations a damping term $-\mu \nabla^6 \zeta$ is included on the right-hand side of Eq. (2.1) to remove energy in the highest wavenumbers and thereby to control aliasing. The coefficient μ is chosen so that waves of wavelength 2Δ have a damping time of two hours, Δ being the grid resolution in both the x and y directions.

Except where otherwise stated, the calculations were carried out with the following parameter values: $\beta = 2.23 \times 10^{-11}\,\mathrm{m^{-1}s^{-1}}$, corresponding with latitude 12.5 degrees; $L =$ 1000 km, giving a domain size 4000 km in the zonal direction and 2000 km in the meridional direction; and with $\Delta = 20$ km. Tests showed that this value of Δ, which is twice as large as that used in Part I, was adequate for the present calculations.

Throughout the paper we have occasion to compare the results with the principal calculation of Part I; namely, the motion of an initially-symmetric vorticity distribution on a beta plane at rest with the foregoing value of β on a square domain $2000 \times 2000\,\mathrm{km}^2$. We shall refer to this as *the standard calculation.*

As noted in section 1, we use the Kasahara–Platzman method for partitioning between 'the vortex' and 'the environment'. In this, the vortex is defined to be the symmetric relative vorticity distribution of the initial vortex, appropriately located, whereupon all the flow change accompanying the vortex motion, including the imposed basic flow, combine to define the vortex environment. We denote the vorticity and streamfunction of the environment by Γ and Ψ, respectively, where $\nabla^2 \Psi = \Gamma$. Henceforth we use ζ to denote the symmetric vorticity distribution ζ_0, consistent with Part I. The position of the relative vorticity maximum is chosen as the location of the vortex centre. For later discussion, it is convenient here to introduce the concept of 'vortex asymmetry'; by this we mean the vortex environment as defined above, minus the initial basic flow. This is characterized by the vorticity field $\Gamma - \overline{\zeta}$, where $\overline{\zeta} = \nabla^2 \overline{\psi}$, and by the streamfunction field $\Psi - \overline{\psi}$.

In section 3 we consider vortex motion in zonal flows with three functional forms and in section 4 we examine motion in flows represented by large-scale, stationary planetary-wave modes of the type expressed by Eq. (2.3) when $U_d = 0$.

3. Vortex motion in a zonal flow

In this section we study vortex motion in three particular zonal shear flows; the first with $\bar{u}(y)$ given by

$$\bar{u}(y) = U'y \tag{3.1}$$

the second with

$$\bar{u}(y) = \tfrac{1}{2}U''y^2 \tag{3.2}$$

and the third with

$$\bar{u}(y) = U\sin(\pi y/2L) \tag{3.3}$$

where U, U' and U'' are constants.

In the case of linear shear (Eq. 3.1) we describe three calculations, referred to as 3A1, 3A2 and 3A3, in which U' has the values $-5 \times 10^{-6}\,s^{-1}$, $5 \times 10^{-6}\,s^{-1}$ and $1 \times 10^{-5}\,s^{-1}$, respectively. As in the standard calculation, these were carried out on a square domain $L \times L$ with $\Delta = 10$ km. According to the results of earlier studies (e.g. Kasahara and Platzman 1963; DeMaria 1985) one would expect the vortex to move with a component of motion in the direction of the zonal flow (where it exists) and with a component in the direction of the absolute vorticity gradient with speed proportional to this gradient. When there is no zonal flow, the vortex has a westward component of motion as well as that in the direction of the absolute vorticity gradient, both being proportional in strength to the value of β (Chan and Williams 1987). It is demonstrated below that for a sufficiently weak westerly flow and positive absolute vorticity gradient, the vortex moves with a component towards the west also. In the foregoing calculations the shear does not contribute to the absolute vorticity gradient of the basic flow, but it does produce a distortion of the vortex asymmetries and accordingly affects the vortex motion.

Figure 1 shows the vortex tracks in the three linear shear calculations for vortices located initially at the origin, where $\bar{u}(0) = 0$, and compares these with the track in the standard calculation. It is evident that positive shear increases the northward motion of the vortex while negative shear decreases it. The question emerges as to whether this tendency may be understood in terms of the effect of shear on the vortex asymmetry and therefore on the streamflow across the vortex centre. We explore this question below.

Figure 2 compares the asymmetric vorticity ($\Gamma - \zeta$) and streamfunction ($\Psi - \bar{\psi}$) fields for the three calculations with those for the standard calculation at 24 hours. Even though the shear is uniform, it has a marked effect on the vortex asymmetry. In the case of positive shear, the vorticity gyres are stronger than in the standard calculation, but on account of the shear, their principal axis (the line joining the asymmetric vorticity maximum and minimum) is displaced poleward relative to the vortex axis. These changes are reflected in the associated streamfunction patterns. Comparison of Figs. 1(e) and 1(g) shows the tendency of shear to extend the vorticity gyres in the zonal direction as might be expected. Calculations of the relative asymmetric streamflow (not shown) confirm that, as in the standard calculation (see Part I, Fig. 8) and in the more general cases considered below (see Figs. 7(d) and 10(b)), the asymmetric flow across the vortex centre acts, to a close approximation, as a steering current for the vortex. This being the case, in the presence of uniform shear, it is evident that the effect of the strengthening

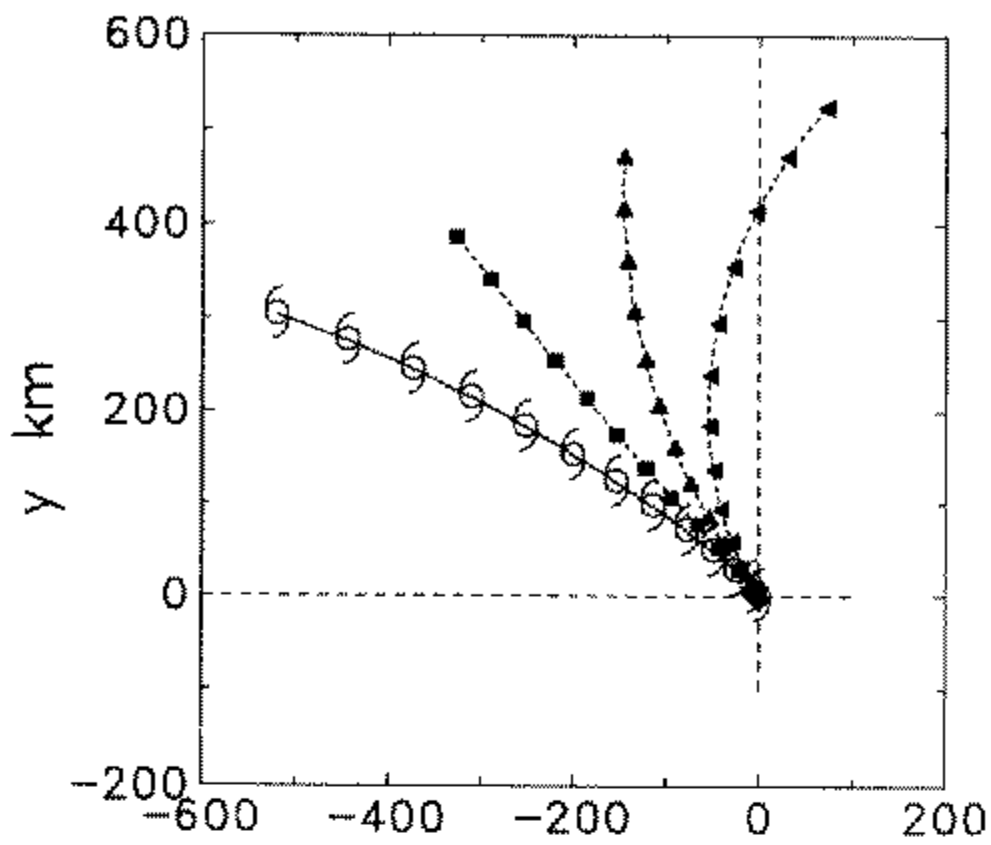

Figure 1. Vortex tracks in cases 3A1, 3A2 and 3A3 where there is a linear basic zonal flow $\bar{u} = U'y$, compared with that in the standard calculation. Vortex positions are indicated each six hours by a cyclone symbol in the standard calculation, by ■ in case 3A1, ▲ in 3A2 and ◀ in 3A3. The tracks begin at the origin.

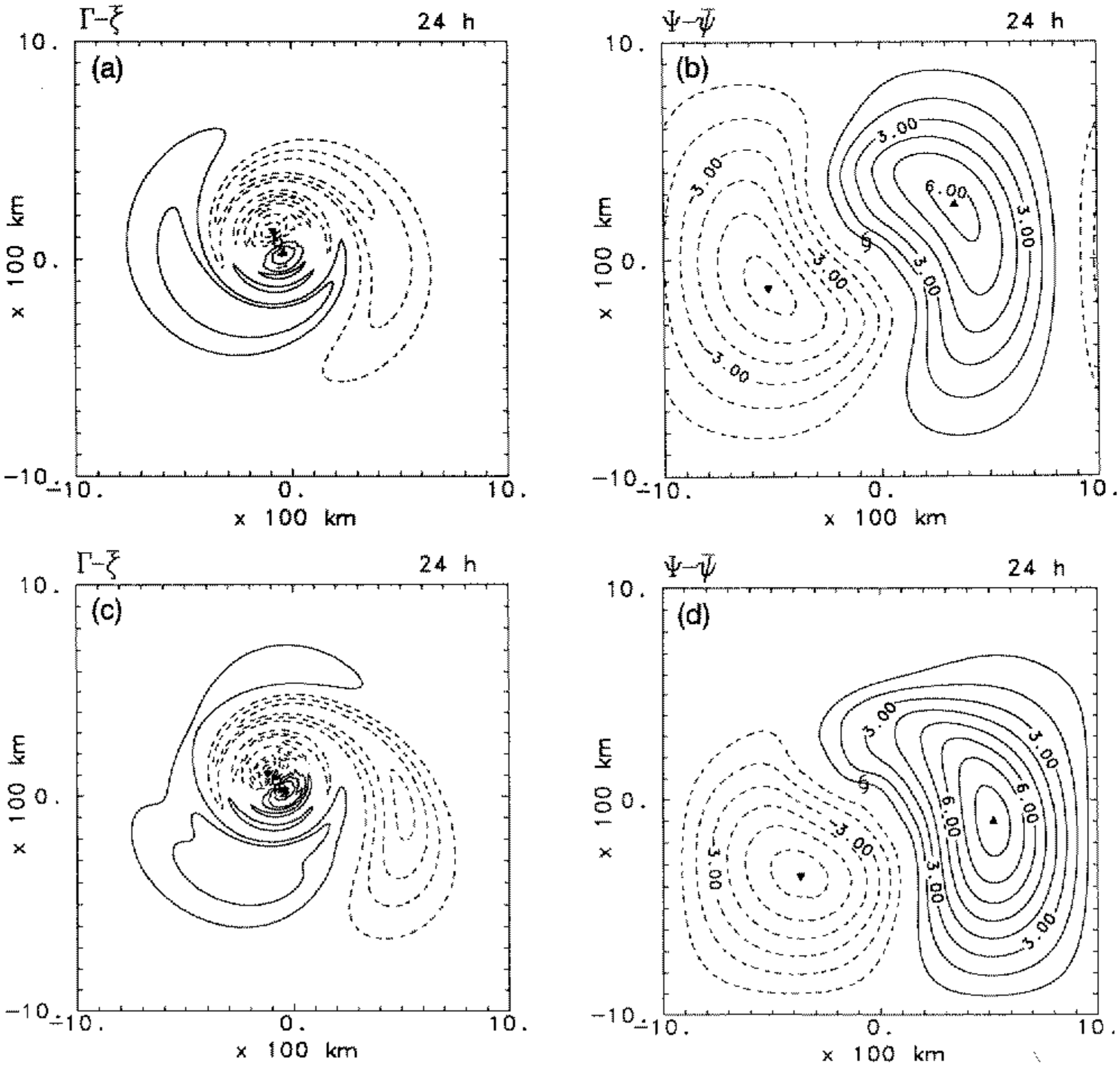

Figure 2. Asymmetric vorticity $\Gamma - \overline{\zeta}$ and asymmetric streamfunction $\Psi - \overline{\psi}$ after 24 hours: (a), (b) in the standard calculation; (c), (d) in calculation 3A1; (e), (f) in 3A2; (g), (h) in 3A3. Contour increment is $5 \times 10^{-6}\,s^{-1}$ for vorticity and $1.0 \times 10^{5}\,m^2\,s^{-1}$ for streamfunction.

of the gyres on the vortex motion is largely offset by the displacement of the vortex centre from the axis of the gyres. In the cases of positive shear studied, the poleward velocity component of the asymmetric flow across the vortex centre is slightly increased, leading to a slightly larger meridional displacement of the vortex (Fig. 1). In the case of negative shear, the gyres are stronger also, but their axis is displaced equatorwards relative to the vortex centre and the net effect is to slightly reduce the meridional speed of the vortex.

The rotation/distortion of the asymmetry has a small effect also on the zonal component of the asymmetric flow in comparison with the standard case, but the effect on the vortex motion is small compared with that of advection by the zonal flow itself.

In the case of quadratic shear (Eq. 3.2) we carried out two main calculations using the same domain size and grid resolution as in calculations 3A1–3A3. The first, referred to as 3B1, is for an f-plane with $U'' = -\beta$, i.e., there is no planetary beta effect, but there is a positive absolute vorticity gradient β associated with the shear flow, itself. This allows us to isolate the effects of pure shear on vortex motion. The second calculation, referred to as 3B2, is on a beta plane with β halved in value and with $U'' = -\frac{1}{2}\beta$. These are compared with the standard calculation. A common feature of these calculations is that the absolute vorticity gradient of the basic state is the same, but the relative contribution to it from the shear varies between the extreme cases of all shear in 3B1 to

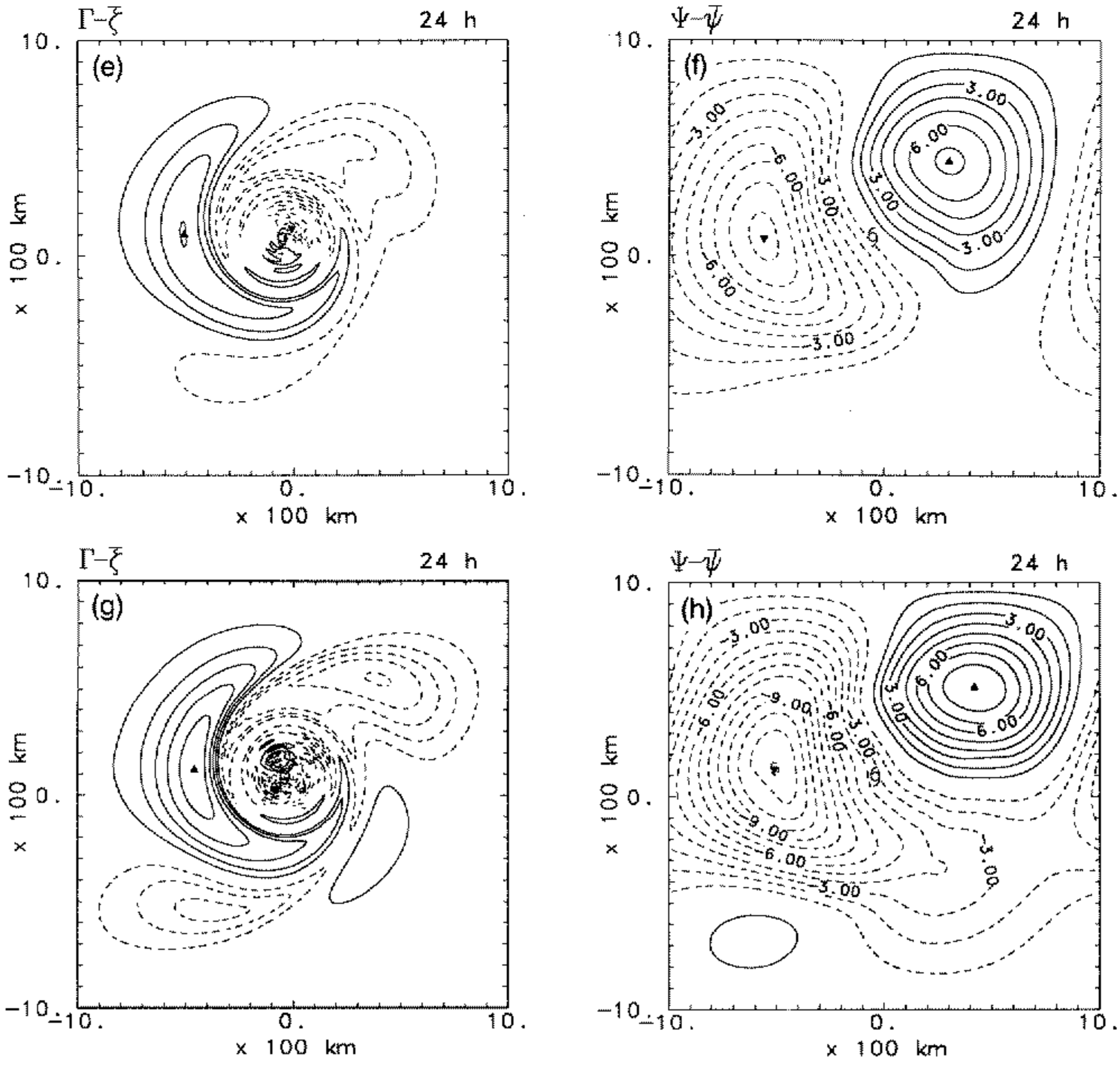

Figure 2. Continued.

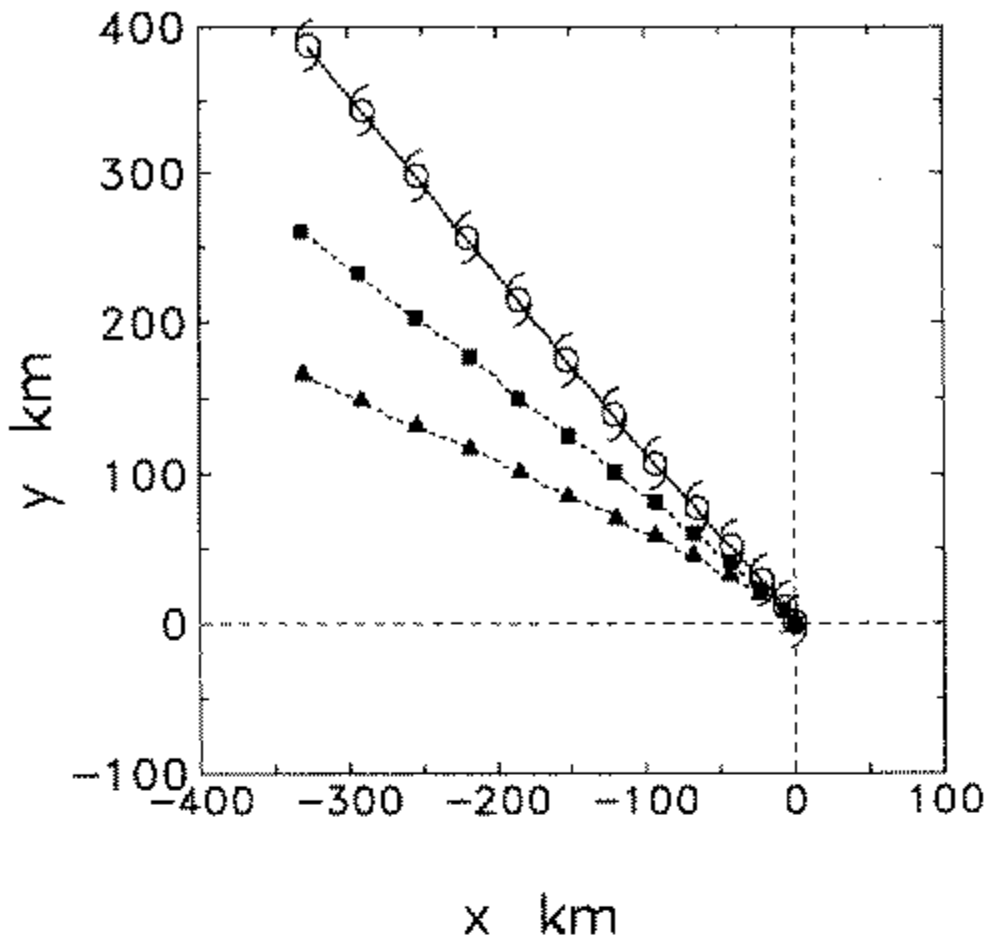

Figure 3. Vortex tracks in cases 3B1 and 3B2 where there is a zonal flow of the form $\bar{u} = \frac{1}{2}U''y^2$, compared with that in the standard calculation. Vortex positions are indicated every six hours by a cyclone symbol in the standard calculation, by ■ in case 3B1 and by ▲ in case 3B2. The tracks begin at the origin.

no shear in the standard calculation. Comparison of results from these calculations enables us to expose the role of non-uniform shear.

Figure 3 shows the vortex track for vortices initially at the origin (where again $\bar{u}(0) = 0$) in these three calculations. In each case, the motion lies in the north-west sector, consistent with the positive absolute vorticity gradient, but the northward displacement is reduced as the magnitude of the basic shear vorticity gradient $|U''|$ is increased. In contrast, the westward displacement barely changes. Again the changes are consistent with changes in the streamfunction asymmetries shown in Fig. 4 at 24 hours. In both cases, the streamfunction gyres are weaker than in the standard calculation and since the vortex remains close to the axis of the gyres, the asymmetric flow across the vortex centre is reduced; it also becomes more westerly. These effects increase with $|U''|$. Calculations show in these cases also that the asymmetric flow at the vortex centre provides an accurate steering current for the vortex. The relationship between the changes in the streamfunction asymmetries and those in the vorticity asymmetries are rather subtle and are best understood in terms of an extension of the analytic theory described in Part 1 and more comprehensively by Smith and Ulrich (1990). A detailed discussion is beyond the scope of the present work and will be published separately in due course. The foregoing results demonstrate elegantly that the relative contribution of the vorticity gradient associated with the shear and that of β to the absolute vorticity gradient is a significant factor in determining vortex motion; not the absolute vorticity gradient alone.

In a further calculation, U'' was taken equal to $-\beta$, which had the same value as in the standard calculation. In this, the gyre structure was similar to that in calculation 3B2, but, as expected, the gyre strength was doubled and the 48-hour vortex displacement was approximately[1] doubled also.

We consider now vortex motion in the zonal shear flow defined by Eq. (3.3) with $U > 0$, the calculation referred to as 3C. Thus U is the westerly wind speed at $y = L$. This flow might be regarded as the limiting case of a stationary planetary wave as the zonal wavelength tends to infinity. The meridional variation of the basic zonal velocity $\bar{u}(y)$; relative vorticity, $\bar{\zeta} = -\mathrm{d}\bar{u}/\mathrm{d}y$; absolute vorticity, $\bar{\zeta}_a(y) = \bar{\zeta}(y) + f$; and absolute

[1] Approximately, because the larger vortex displacement results in a larger influence of the northern channel boundary at later times.

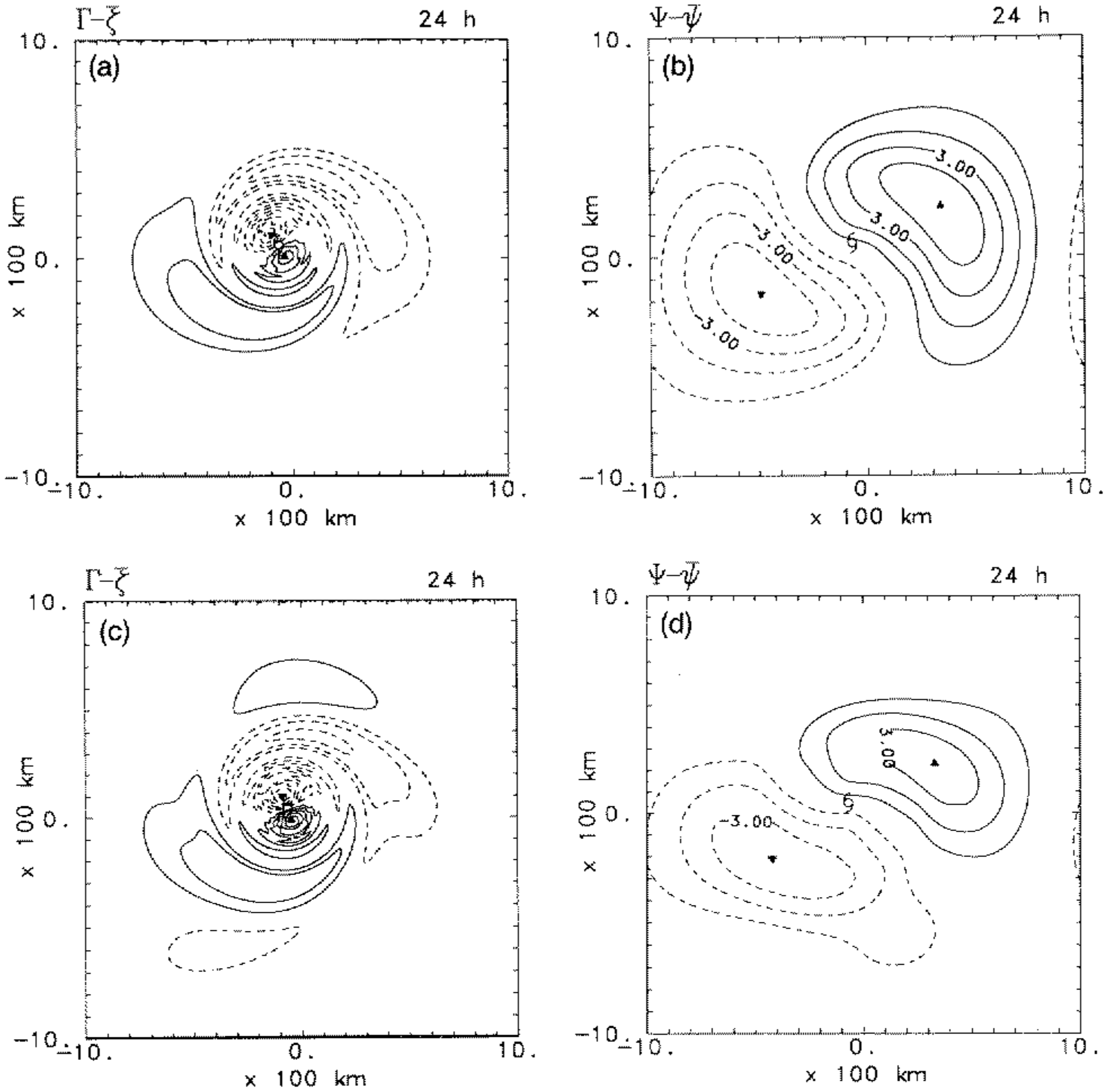

Figure 4. As for Fig. 2, except (a), (b) for calculation 3B1; (c), (d) for 3B2.

vorticity gradient, $d\bar{\xi}_a/dy = d\bar{\xi}/dy + \beta$, are shown in Fig. 5 for the value $U = 10\,\mathrm{m\,s^{-1}}$. Note that the zonal winds are easterly for $y < 0$ and westerly for $y > 0$. Moreover, the relative vorticity is maximum anticyclonic at $y = 0$ whereupon the x-axis corresponds with the subtropical ridge in the atmospheric situation.

Using Eq. (3.3),

$$\frac{d\bar{\xi}_a}{dy} = \beta + (\pi/2L)^2 U \sin(\pi y/2L) \tag{3.4}$$

whence, for $U > 0$, $d\zeta_a/dy \geq 0$ for $y \geq 0$. However, if $U > u_c = \beta(2L/\pi)^2$, there is a region $-L \leq y \leq y_c$, where $y_c = -(2L/\pi)\ \sin^{-1}(u_c/U)$, in which $d\bar{\zeta}_a/dy < 0$. For the parameters used here, $u_c = 9.0\,\mathrm{m\,s^{-1}} < U$, whereupon the absolute vorticity gradient is negative for $y < y_c = -718\,\mathrm{km}$. For vortices located outside this region, one may expect the vortex track to be insensitive to small changes in the initial vortex position (DeMaria 1985).

Figure 6 shows the vortex track for a vortex located initially in the easterly flow at $x = 0$, $y = -100\,\mathrm{km}$, together with the streamlines of the basic flow and absolute vorticity

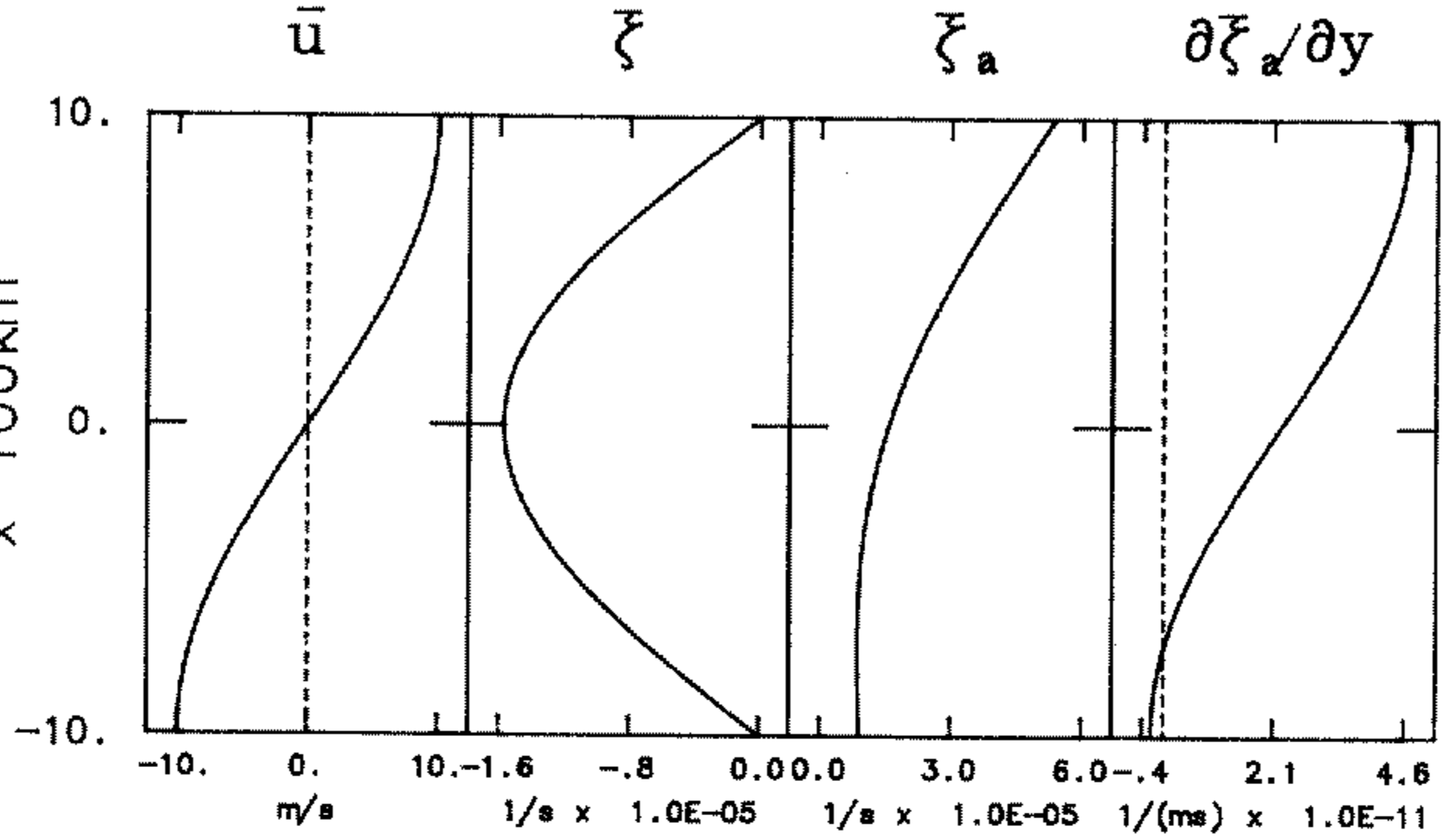

Figure 5. Meridional profiles of zonal velocity $\bar{u}$ ($\mathrm{m\,s^{-1}}$), relative vorticity $\bar{\zeta}$ ($10^{-5}\,\mathrm{s^{-1}}$), absolute vorticity $\bar{\zeta}_a$ ($10^{-5}\,\mathrm{s^{-1}}$) and absolute vorticity gradient $\partial\bar{\zeta}_a/\partial y$ ($10^{-11}\,\mathrm{m^{-1}\,s^{-1}}$) for calculation 3C.

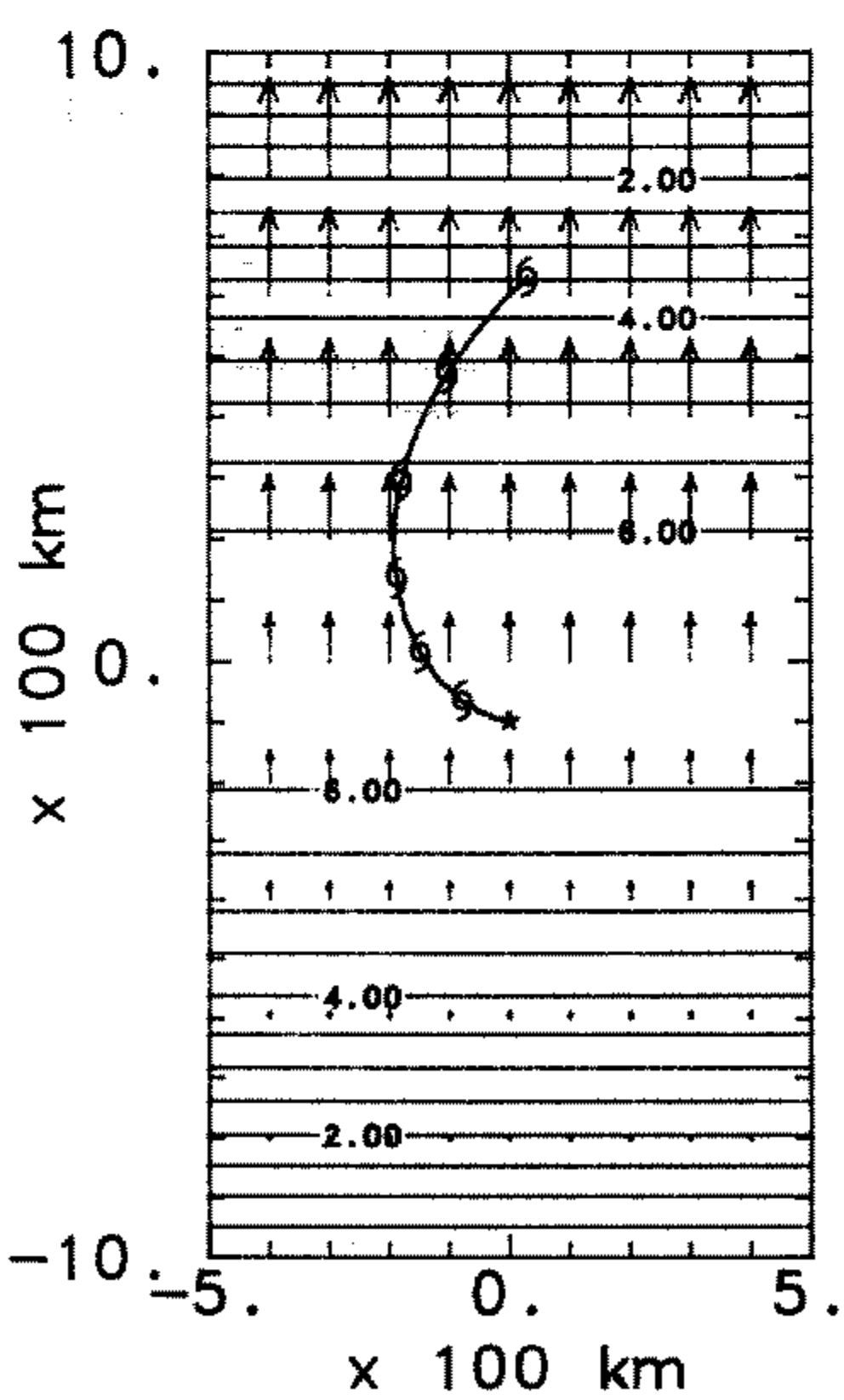

Figure 6. Vortex track in calculation 3C. Horizontal lines are streamlines (units $10^6\,\mathrm{m^2\,s^{-1}}$). Arrows denote the absolute vorticity gradient vector, the magnitudes of which may be found in Fig. 5. Cyclone symbols mark the vortex positions at 12-hour intervals. The initial vortex position is (0, −100)km.

gradient vectors. Again, consistent with the results of earlier studies it can be shown that the vortex moves with a component in the direction to the left of the absolute vorticity gradient, its speed in this direction increasing with the magnitude of the gradient. Thus, initially the track is west-north-westwards, but becomes more northerly and later north-easterly as the vortex recurves into the westerlies. Moreover, it is evident that in all flow configurations of this general type, with westerly flow to the north, easterly flow to the south and positive absolute vorticity gradient in between, recurvature of the vortex is inevitable. The asymmetric vorticity field at 24 hours (Fig. 7(a)) is similar to that in case 3A3 (see Fig. 2(g)), suggesting that the distortion of the gyre, in comparison with the standard calculation, is dominated by the linear shear contribution. This, together with the fact that the vortex moves into a field of increasing absolute vorticity gradient explains why the total northward displacement after 72 hours is greater than in the standard case.

Figure 7(b) shows the environmental streamfunction at 24 hours, with the location of the vortex centre at this time. Note that the presence of the vortex leads to a significant change in the structure of the subtropical ridge. This change can be attributed to the

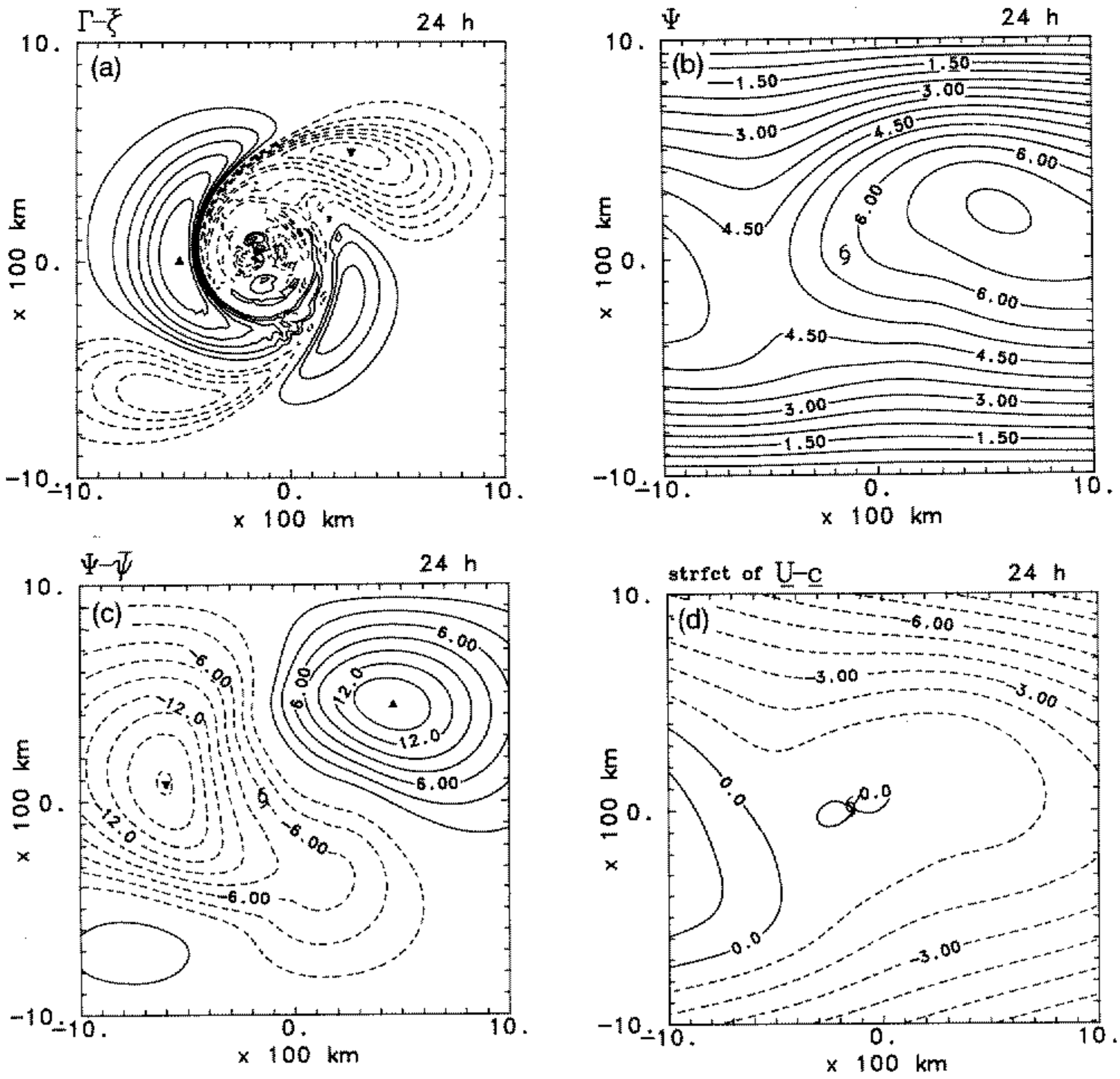

Figure 7. Flow characteristics of calculation 3C in the central half of the domain at 24 hours: (a) asymmetric vorticity field $\Gamma - \bar{\zeta}$ (units $10^{-5}\,s^{-1}$, contour interval $5.0 \times 10^{-6}\,s^{-1}$); (b) environmental streamfunction Ψ (units $10^6\,m^2\,s^{-1}$ and with contour interval 5.0 units); (c) streamfunction of the vortex asymmetry $\Psi - \bar{\psi}$ in the same units as (b), but with the contour interval 2.0 units; (d) environmental streamfunction relative to the vortex motion with units as in (c) and contour interval 1 unit. The centre of the symmetric vortex is marked by a cyclone symbol. Note that the distortion from the original zonal flow structure in (b) and the region of weak relative streamfunction gradient across the vortex in (d).

development of a pair of counter-rotating gyres as in earlier cases. However, the gyres are overshadowed by the streamfunction of the zonal flow and their presence is revealed only if the latter is removed (Fig. 7(c)). This result has implications for the detection of the β-gyres from observational data within the tropical cyclone environment. It suggest that the gyres may be readily observable only if the large-scale flow is sufficiently weak.

Figure 7(d) shows the streamfunction of the environmental flow relative to the vortex motion at 24 hours. It is apparent that the relative velocity is small over the inner few 100 km of the vortex and therefore, as in the standard case, the asymmetric flow across the vortex centre provides an accurate 'steering current' for the vortex motion.

4. Vortex motion in a stationary planetary wave

We consider now vortex motion in a large-scale stationary planetary wave described by Eq. (2.3) with $U_d = 0$. Then from Eq. (2.4), $U = 2\beta L^2/\pi^2 = 4.4\,\mathrm{m\,s^{-1}}$. The wave amplitude characterized by $\hat{\psi}/L$ is $3.3\,\mathrm{m\,s^{-1}}$. Figure 8 shows the streamlines corresponding to this wave together with the absolute vorticity gradient vectors, $\nabla\bar{\zeta}_a$. For the parameters chosen, the wave has an anticyclonic centre in the south and a cyclonic centre in the north, with easterly flow equatorwards of the anticyclone (and polewards of the cyclone). To suggest an analogy with the situation in the atmosphere, we shall refer to the anticyclone as 'the subtropical anticyclone', but we have retained the tropical value of β used previously to afford comparison with earlier calculations. Since β at 25 degrees latitude is 93% of β at 12.5 degrees, this does not lead to gross inaccuracy. However, one must bear in mind that the scale of the anticyclone in the model is relatively small compared with the typical subtropical anticyclone.

Note that the vectors $\nabla\zeta_a$ have significant departures from a meridional orientation in certain parts of the wave; in particular the meridional component is negative south of the subtropical anticyclone which is centred near ($x = 250\,\mathrm{km}$, $y = -300\,\mathrm{km}$). More generally, the anticyclonic region is one in which $\nabla\cdot(\nabla\bar{\zeta}_a) = \nabla^2\bar{\zeta}_a < 0$, whereupon, according to the results of DeMaria (1985), the vortex track for a vortex initialized in this region will be sensitive to small changes in the initial position.

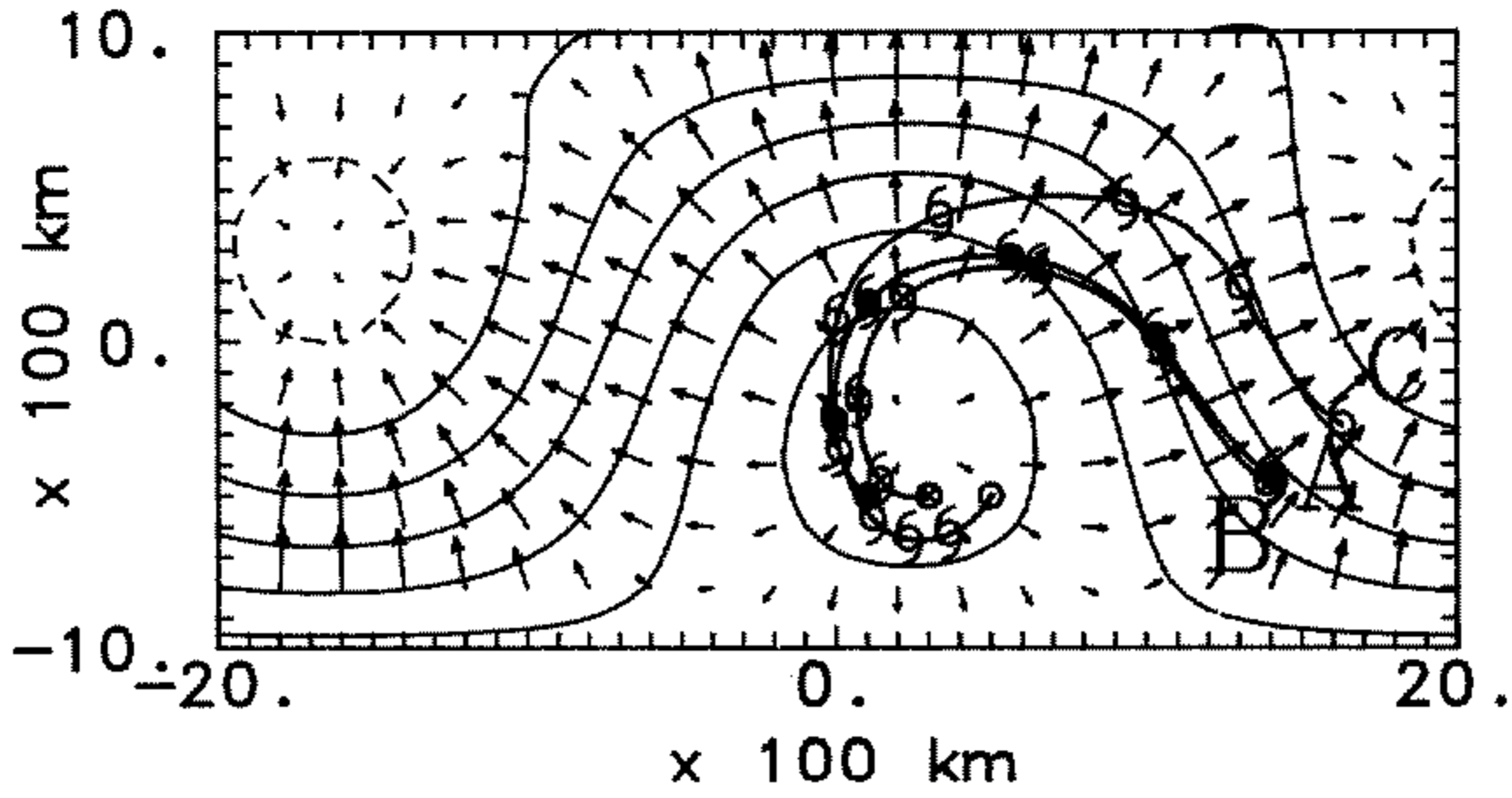

Figure 8. Vortex tracks for calculations 4A, 4B and 4C. The initial vortex positions of A, B and C are (100, −500), (300, −500) and (500, −500) in km, respectively. Arrows denote the absolute vorticity gradient vector (maximum arrow length corresponds to a gradient of $7.3 \times 10^{-11}\,\mathrm{m^{-1}\,s^{-1}}$). Cyclone symbols mark the vortex position at 24-hour intervals.

Shown also in Fig. 8 are the tracks of three vortices, each located initially in the subtropical easterlies (at $y = -500$ km), but displaced zonally at $x = 100$ km, $x = 300$ km and $x = 500$ km. We refer to these calculations as 4A, 4B and 4C, respectively. On the whole all three tracks are similar, showing eventual recurvature into the westerlies and interestingly, long-term integration (to 480 hours) shows that the demise of all three model vortices occurs in the region of the cyclone centre of the planetary wave (where $\nabla\bar{\zeta}_a$ is convergent). Although this particular situation is not of immediate relevance to the atmospheric situation, the latter result points to the tendency of a large-scale cyclone centre to act as an attractor of smaller-scale vortices. The result, itself, is of relevance, for example to the case of interaction between a large tropical cyclone vortex and a smaller one, a situation that is common in the tropical north-west Pacific region. Evidently, the reverse is true of a large-scale anticyclone centre.

It is instructive to decompose the vortex motion in these calculations into a component due to advection by the basic flow together with a drift vector related to the absolute vorticity gradient of the basic flow, $\nabla\bar{\zeta}_a$. Specifically we define unit vectors $\hat{\mathbf{a}} = (\nabla\bar{\zeta}_a/|\nabla\bar{\zeta}_a|)_0$ and $\hat{\mathbf{b}} = \hat{\mathbf{k}} \times \hat{\mathbf{a}}$, where $\hat{\mathbf{k}}$ is the unit vector in the vertical direction and the subscript zero denotes the vortex centre. Then, provided $|\nabla\bar{\zeta}_a|_0 \neq 0$, the drift of the vortex relative to the basic current can be expressed by the vector

$$\mathbf{c} - \bar{\mathbf{u}}_0 = A(t)\hat{\mathbf{a}} + B(t)\hat{\mathbf{b}} \tag{4.1}$$

where A and B are functions of time specific to the initial symmetric vortex profile. The variation of A and B with time for the calculation 4B are shown in Fig. 9, together with the variation of $|\nabla\zeta_a|$. During the first 36 hours, $A(t) < 0$ and the vortex moves with a drift component in a direction opposite to the absolute vorticity gradient. During this period it runs into a decreasing absolute vorticity gradient (Fig. 9(b)). At later times this component of drift reverses in sign and at 60 hours increases with the absolute vorticity gradient. Thereafter, it stabilizes at a value of around 2.5 m s^{-1} until 90 hours, when it begins to decrease. The drift component at right angles and to the left of the absolute vorticity gradient is positive, except for the period between 24 and 48 hours, and its magnitude after 40 hours increases steadily to about 4.7 m s^{-1} at 110 hours, after which it begins to decline. It is clear from these diagrams that, unlike the case of zero basic flow in which $\nabla\zeta_a = (0, \beta, 0)$, the coefficients A and B do not evolve in simple proportion to each other; indeed they do not even keep the same sign.

Figure 9(c) shows the ratios of drift speed/vortex speed and vortex speed/mean-flow speed as functions of time. It is striking that, at all stages, the drift speed is more than 20% of the vortex speed and between 60 and 120 hours it is more than 70% of it. On the other hand, the basic flow exceeds the vortex speed, except during the period between 25 and 55 hours, and after 70 hours it is more than 50% greater.

The results for calculations 4A and 4C are broadly similar, but the tracks are a little different because of the different initial positions. In particular, the track in 4C goes initially southwestwards into an increasing easterly component of the basic flow while the track in 4B goes initially westwards and that in 4A initially north-westwards. The tracks in 4A and 4B ultimately converge, but the large initial deviation between these and that in 4C remains permanent.

Figure 10(a) shows the environmental streamfunction in the case 4B at 48 hours when the vortex is close to the centre of the computational domain. Note that there is little apparent distortion of the basic planetary wave, in contrast to the distortion of the basic flow in case 3C. In this case, the gyre structure that emerges when the basic state streamfunction is removed (Fig. 10(c)) serves to broadly reinforce the basic state pattern. As in previous cases, the relative streamfunction of the environmental flow has weak

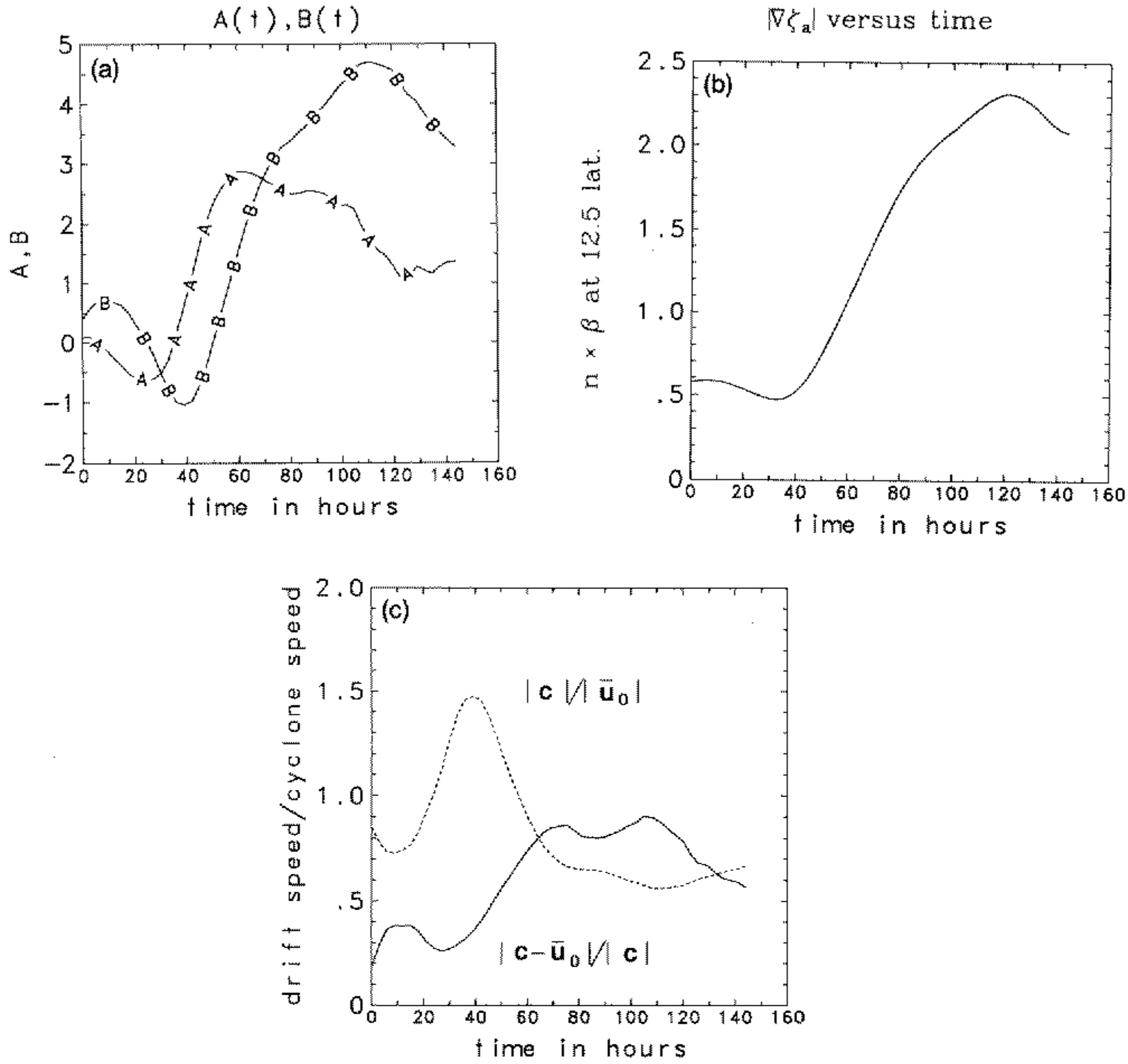

Figure 9. Time series of: (a) the coefficients A(t) and B(t) in Eq. (4.1) for calculation 4A. Units are m s^{-1}; (b) $|\nabla\zeta_a|_0$ in units of β at 12.5 degrees latitude; (c) ratios $|\mathbf{c} - \bar{\mathbf{U}}_0|/|\mathbf{c}|$ (solid line) and $|\mathbf{U}_0|/|\mathbf{c}|$ (broken line) for the same calculation.

gradients across the vortex at several hundred kilometres from its centre as typified by the pattern at 48 hours shown in Fig. 10(b), and the environmental streamflow across the vortex centre provides the steering flow for the vortex, a feature that we return to in section 5.

As in case 3C, the so-called beta gyres are not discernible until one removes the initial basic state (Fig. 10(c)), whereupon a distorted dipole structure emerges. Significantly, this is comparable in scale with the planetary wave itself. The corresponding gyres in the vorticity field are rather more complicated in structure (Fig. 10(d)) reflecting the shearing effect of both the basic state and the tangential wind field of the vortex on the overall vorticity field.

Figures 10(e) and 10(f) show the vortex asymmetries at 72 hours, after the vortex has recurved. Again, the streamfunction gyres (Fig. 10(e)) show a distorted dipole structure but the axis of the gyres has rotated counterclockwise, indicating a larger westward contribution to the vortex motion relative to the basic flow. Comparison of the vorticity asymmetries at 48 and 72 hours (Figs. 10(d) and 10(f)) illustrates the shearing effect of the basic state which is most pronounced at large distances (4–5 times the radius of maximum tangential wind) from the vortex centre where the gyre structure is more

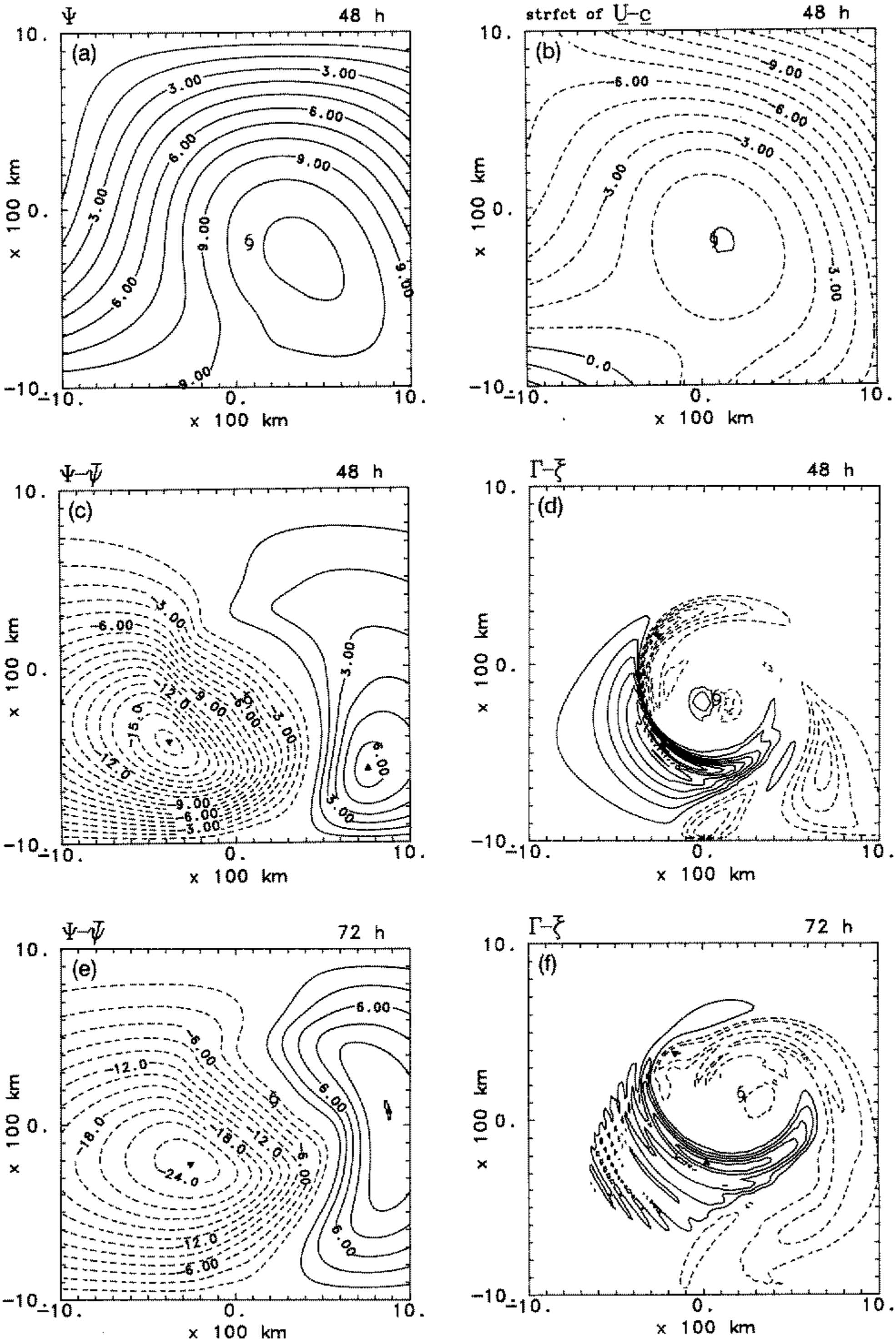

Figure 10. Flow characteristics of calculation 4B in the central half of the domain at 48 hours: (a) environmental streamfunction; (b) environmental streamfunction relative to the vortex motion—both with units $10^6\ m^2\ s^{-1}$ and contour interval 1 unit. The centre of the symmetric vortex is marked by a cyclone symbol at 24-hour intervals; (c) streamfunction of the vortex asymmetry $\Psi - \psi$ (units $10^5\ m^2\ s^{-1}$ and contour interval 1 unit); (d) asymmetric vorticity field $\Gamma - \zeta$ corresponding with (c) (contour interval $5 \times 10^{-6}\ s^{-1}$); (e) $\Psi - \psi$ at 72 hours (contour interval $2.0 \times 10^6\ m^2\ s^{-1}$); (f) $\Gamma - \zeta$ at 72 hours (contour interval $1.0 \times 10^{-5}\ s^{-1}$).

regular. As in the standard vortex calculation, the large radial shear of the tangential wind is effective in homogenizing the inner field, as discussed in Part I and by Carr and Williams (1989) and Shapiro and Ooyama (1990).

It is of theoretical interest to consider the effect of halving the domain size in the zonal direction to 2000 km. This reduces the westward phase speed of the planetary wave relative to the basic current necessary to keep it stationary (now from Eq. (2.4), $U = 1.8\,\mathrm{m\,s^{-1}}$), but increases the horizontal component of $\nabla\bar{\zeta}_a$. Figure 11 shows the track of a vortex located initially south-south-east of the subtropical anticyclone centre. In this case, which we refer to as calculation 4D, the drift associated with the westward-oriented absolute vorticity gradient to the west of the subtropical anticyclone is significant in comparison with the southerly advecting winds there. As a result the vortex tracks north-westwards, again ending in the cyclone centre of the planetary wave, but this time from the east.

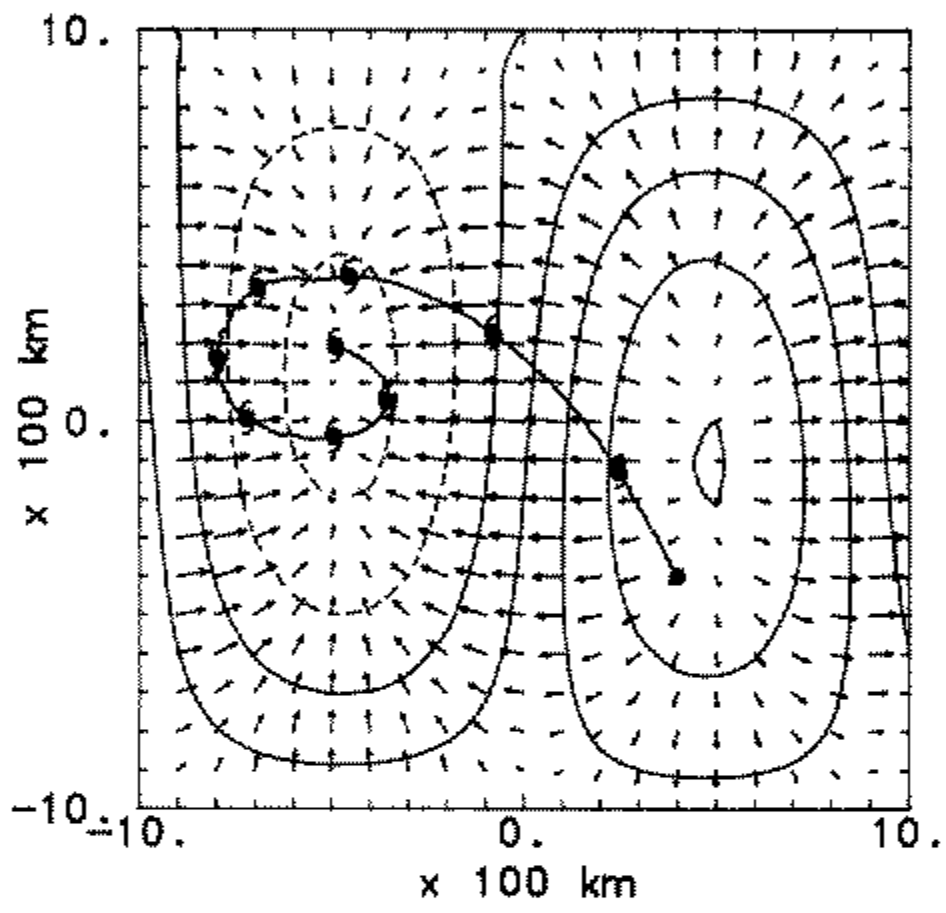

Figure 11. Vortex track in calculation 4D. The initial vortex position is (400, −400) and the contour interval is $2.0 \times 10^6\,\mathrm{m^2\,s^{-1}}$. Other details as for Fig. 6 except maximum arrow length corresponds to an absolute vorticity gradient of $2.8 \times 10^{-10}\,\mathrm{m^{-1}\,s^{-1}}$.

It is clear that the planetary waves of this section are not totally realistic in relation to the mean conditions that obtain in the tropical atmosphere, but we may not suppose that the size of the absolute vorticity gradients associated with them are atypical of those that occur in the *environment* of individual tropical cyclones (those that occur on the vortex scale, as in the model, may be much larger, but in the model they are not coherent and should not be considered relevant to the larger-scale gradient responsible for the beta gyres). At the present time, reliable data of this type appear to be unavailable. Nevertheless, our calculations provide a scenario in which recurvature versus non-recurvature might be understood. Indeed they are strongly suggestive that whether or not recurvature occurs depends on the relative strength and orientation of the basic large-scale flow and on the absolute vorticity gradient associated with it. This ought to provide a testable hypothesis for future field experiments.

5. Estimation of vortex speed and direction

As discussed in Part I, the general paucity of data in and around tropical cyclones precludes the possibility of determining the environmental flow across the vortex centre with the degree of precision afforded by the foregoing numerical simulations. Thus in order to define an environmental current from observed wind data, it is necessary to

average over a considerable area surrounding the cyclone. For example, George and Gray (1976) use an average over an annular region 1–7 degrees latitude in radial extent centred on the cyclone, while Chan and Gray (1982) use an annular region from 5–7 degrees latitude. As in Part I, the present calculations provide an effective means of assessing the applicability of these or other averages in defining an appropriate environmental current. Therefore we have again calculated the environmental wind vector averaged over annular regions from 0–1, 1–3, and 3–5 degrees latitude, centred on the vorticity centre, and have compared these with the environmental flow calculated at the vorticity centre, and with the speed of the centre itself. The centre-finding procedure is described in Part I. We were unable to consider a 5–7 degrees latitude annulus on account of the restricted size of the computational domain. The results are similar in all cases and are typified by those for the calculation 4B shown in Fig. 12. This shows the speed (Fig. 12(a)) and direction (Fig. 12(b)) as time series calculated by

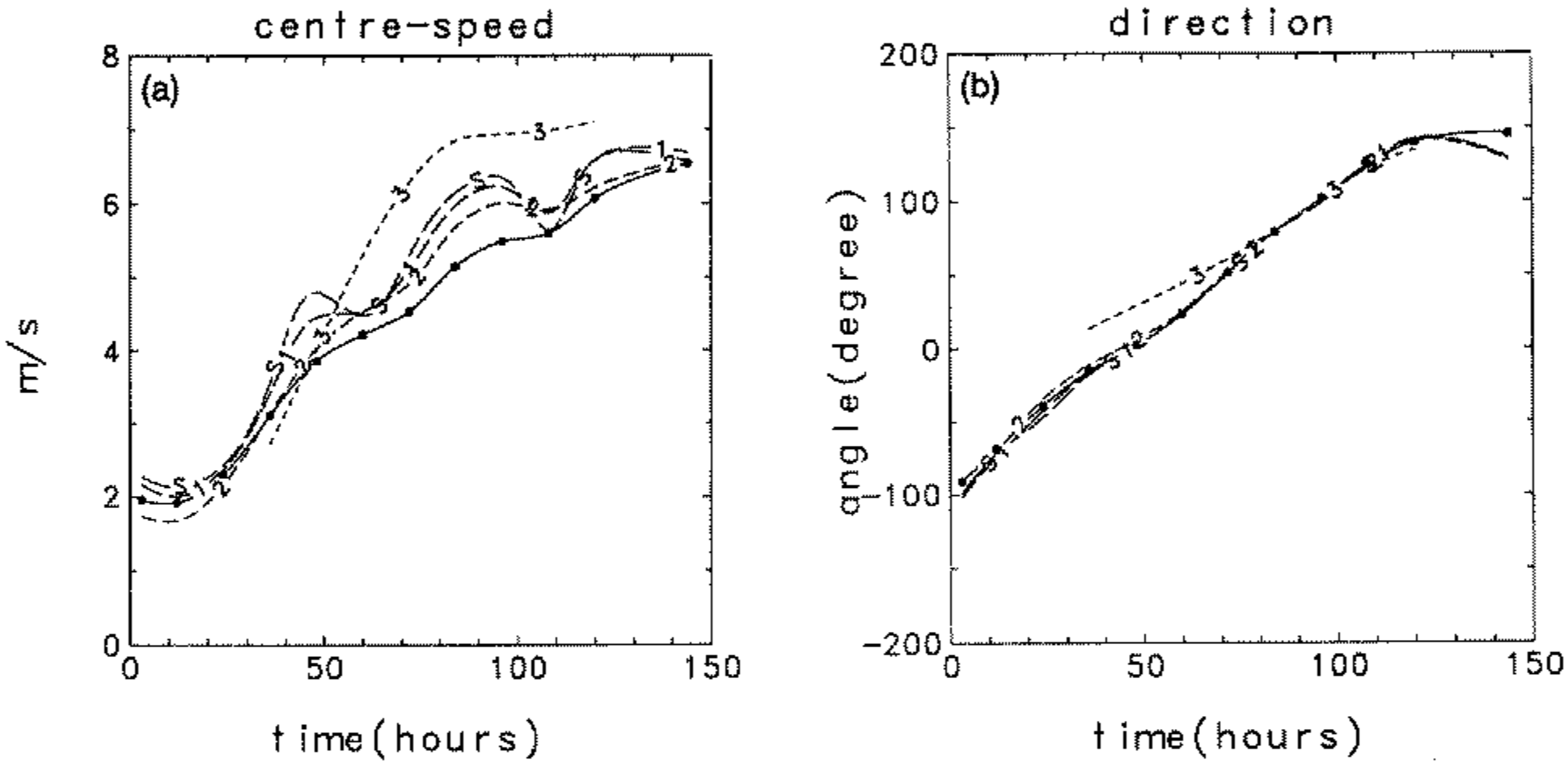

Figure 12. Time series of vortex centre speed (a), and direction (b) in calculation 4B. The speed and direction are calculated using centred differences on the position of the relative vorticity maximum at 24-hourly intervals and are denoted by the thick black line joining dots, the first two at 6 and 12 hours and subsequent ones at 24-hour intervals. The lines marked 1, 2 and 3 are speeds calculated by averaging the environmental flow over a circular region of radius 1 degree from the vortex centre, and over annular rings from 1–3 degrees and 3–5 degrees, respectively. The latter curve is omitted at times when the vortex moves within less than 5 degrees of the meridional boundaries.

various methods, compared with the speed of the vorticity maximum, denoted by the thick black line joining dots at 12-hour intervals. This centre speed and direction are calculated using centred differences on the location of the vortex centre at 24-hour intervals. The lines marked 1, 2 and 3 are speeds calculated by averaging the environmental flow over a circular region of radius 1 degree from the vortex centre, and over annular rings from 1–3 and 3–5 degrees, respectively. The latter curve is omitted at times when the vortex moves within less than 5 degrees of the meridional boundaries. The results are a little different from those in Part I. While the directions produced by all methods are relatively close, the speed calculated from the environmental streamfunction is slightly worse than the inner averages (0–1 and 3–5 degrees). The outermost average is least accurate, as in the standard case. It is likely that the difference between the measured speed and that calculated from the streamfunction is largely a reflection of the coarser resolution used in the present calculation in comparison with the standard calculation. The inner two averages are more accurate when there is a basic flow, because of the relatively smaller contribution of the vortex asymmetries.

6. Effects of domain size

Perhaps the most serious limitation of the foregoing calculations is the restricted domain size in the meridional direction. Fiorino (1987) has explored this question in detail for the standard case and has shown that a domain size of $2000 \times 2000\ \text{km}^2$ is too small for an accurate track prediction after 24 hours, presumably because the vortex begins to have significant interaction with the boundary beyond this time. However, in using a larger domain, Fiorino compromises resolution by choosing a grid size of 40 km. While this seems to be adequate for track prediction, we noted in Part I that it is inadequate for a calculation of the vorticity field. For this reason, we have used a reduced grid size of 20 km. Furthermore, the inclusion of a zonal flow necessitated a larger domain in the zonal direction to prevent vortex asymmetries 're-entering' the domain as a result of the periodic boundary conditions. We have found it necessary, therefore, to restrict the meridional domain size to 2000 km. However, we have carried out one calculation, similar to 4B, but with the meridional domain size increased to 4000 km (Fig. 13). While interesting in its own right, this does not allow one to assess completely the limitations of the smaller domain because the parameter values for the large-scale flow are necessarily changed also; i.e., the particular value of U for which $U_d = 0$ in Eq. (2.4) is increased to $7.2\ \text{m s}^{-1}$. In the calculation we chose the amplitude of the planetary wave, characterized by $\hat{\psi}/L$, to be $12.7\ \text{m s}^{-1}$. In this case, the vortex track follows the streamlines of the basic flow more closely as the relative effect of advection on the motion is increased in magnitude, but despite this, after recurvature the vortex again tracks towards the cyclonic centre of the planetary wave. Like the previous cases, the vortex speed is generally less than the speed of the basic flow, but mostly not more than 20% less, and again the coefficients A and B in Eq. (4.1) are mostly, but not always, positive.

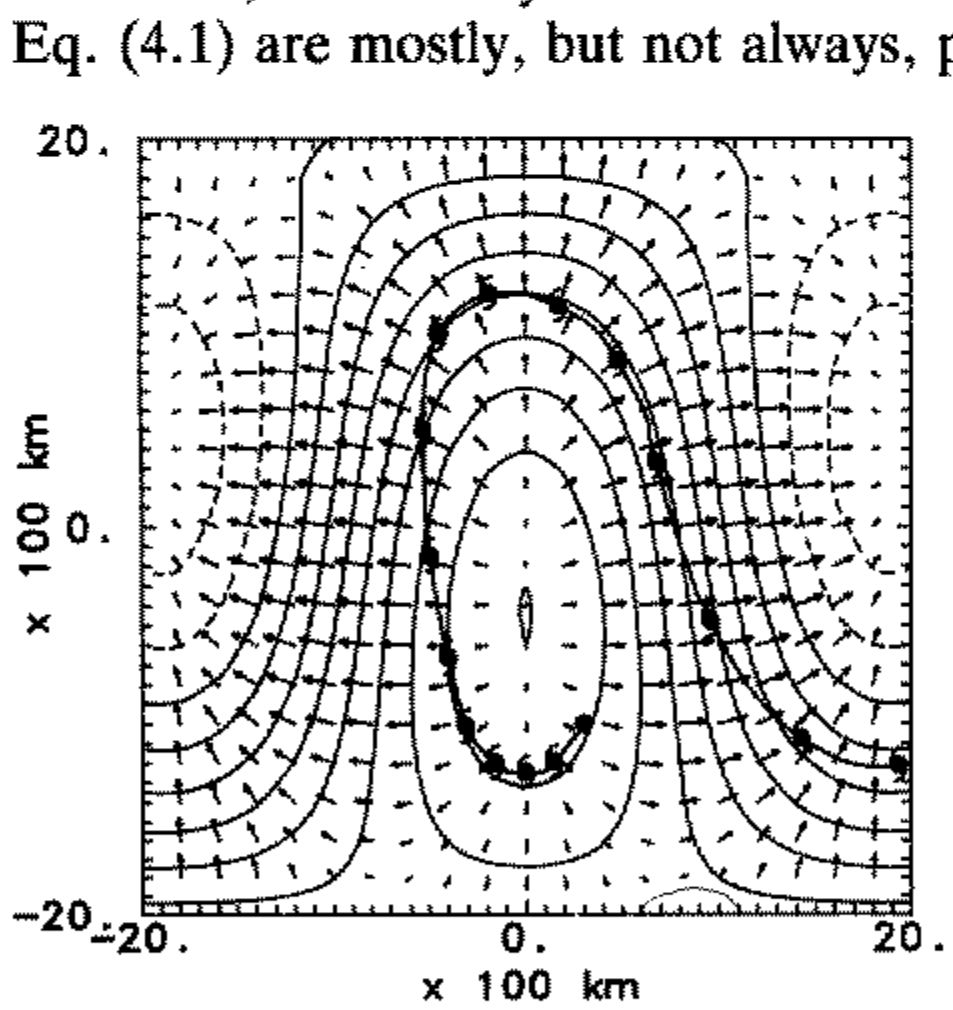

Figure 13. Vortex track, streamline pattern and absolute vorticity gradient vectors for the planetary wave calculation with a $4000 \times 4000\ \text{km}^2$ domain size. Cyclone symbols mark the vortex position every 6 hours. The initial vortex position is (500, −1000) km. Arrows denote the absolute vorticity gradient vector with maximum arrow length corresponding to a gradient of $1.4 \times 10^{-10}\ \text{m}^{-1}\,\text{s}^{-1}$.

7. Conclusions

The foregoing calculations extend our study in Part I of vortex motion on a beta plane to motion in spatially-varying large-scale flows. They highlight the role of vortex asymmetries, analogous to the beta gyres, in producing motion relative to the basic flow. In particular, in a uniform zonal shear flow they point to two competing processes affecting vortex motion: differential advection of the evolving vorticity asymmetries by

the basic shear tends to increase the overall strength of the associated asymmetric circulation, but the distortion of the gyres leads to a displacement of the gyre axis relative to the vortex centre. As a result, the meridional component of vortex motion is little changed. However, shear has a major impact on the vortex track because of advection by the basic flow itself.

Nonuniform zonal shear leads to a change in the gyre strength, in part through its contribution to the absolute vorticity gradient seen by the vortex and in part because of its distorting effects on the vortex vorticity and the vortex asymmetry. However, vortex motion cannot be characterized by the basic-state absolute vorticity gradient alone—the proportionate contribution of the shear to the absolute vorticity gradient is important also.

In all the basic flows considered, the environmental flow across the vortex centre provided an accurate steering current for the vortex. Furthermore, the vortex asymmetries were concealed by the presence of the basic flow and they became apparent only when the latter was removed. It follows that the so-called beta gyres may be exceedingly difficult to observe in nature.

In the case of vortex motion in the spatially-varying basic flow provided by a finite amplitude planetary wave, the drift speed of the vortex relative to the basic flow accounted for a significant fraction (up to 60%) of the total motion. Again, there is no simple relationship between the local absolute vorticity gradient of the basic flow and the vortex motion relative to the basic flow.

In a zonal basic flow with westerlies poleward of easterlies and a positive absolute vorticity gradient, recurvature of a vortex initially in the easterlies is inevitable. However, a sufficiently large east–west gradient of absolute vorticity in the vortex environment can inhibit or prevent recurvature. In reality, a suitable gradient might be associated with a synoptic-scale trough or even a larger neighbouring tropical cyclone, for example.

Averaging the environmental flow over annuli centred on the storm to evaluate the storm-motion vector is a more accurate procedure in the presence of a basic flow, although an average over a 3–5 degrees latitude annulus gives relatively poor results compared with a 1–3 degrees latitude annulus.

Acknowledgement

Our thanks go to Gudrun Fingerle who capably prepared the original and revised versions of this manuscript and several drafts of it in between.

The research was supported by the US Office of Naval Research.

References

Carr, L. E. and Williams, R. T. 1989 Barotropic vortex stability to perturbations from axisymmetry. *J. Atmos. Sci.*, **46,** 3177–3191.

Chan, J. C. L. and Gray, W. M. 1982 Tropical cyclone movement and surrounding flow relationships. *Mon. Weather Rev.*, **110,** 1354–1374

Chan, J. C. L. and Williams, R. T. 1987 Analytical and numerical studies of the beta-effect in tropical cyclone motion. Part I: Zero mean flow. *J. Atmos. Sci.*, **44,** 1257–1265

DeMaria, M. 1985 Tropical cyclone motion in a nondivergent barotropic model. *Mon. Weather Rev.*, **113,** 1199–1210

Elsberry, R. L. 1987 Tropical cyclone motion. In *A global view of tropical cyclones*. Ed. R. L. Elsberry. Office of Naval Research, Washington, DC

Fiorino, M. 1987 'The role of vortex structure in tropical cyclone motion'. Ph.D. Thesis. Naval Postgraduate School, Monterey, California

Fiorino, M. and Elsberry, R. 1989 Some aspects of vortex structure related to tropical cyclone motion. *J. Atmos. Sci.*, **46**, 975–990

George, J. E. and Gray, W. M. 1976 Tropical cyclone motion and surrounding parameter relationships. *J. Appl. Meteorol.*, **15**, 1252–1264

Kasahara, A. and Platzman, G. W. 1963 Interaction of a hurricane with a steering field and its effect upon the hurricane trajectory. *Tellus*, **15**, 321–335

Shapiro, L. J. and Ooyama, K. 1990 Barotropic vortex evolution on a beta plane. *J. Atmos. Sci.*, **47**, 170–187

Smith, R. K. and Ulrich, W. 1990 An analytical theory of tropical cyclone motion using a barotropic model. *J. Atmos. Sci.*, **47**, 1973–1986

Smith, R. K., Ulrich, W. and Dietachmayer, G. 1990 A numerical study of tropical cyclone motion using a barotropic model. I: The role of vortex asymmetries. *Q. J. R. Meteorol. Soc.*, **116**, 337–362